Title

Stopped-Flow Kinetic Investigations of the Activation of Soybean Lipoxygenase-1 and the Influence of Inhibitors on the Allosteric Site †

Journal

Biochemistry, 42(14)

ISSN

0006-2960

Authors

Ruddat, Viola C
Whitman, Stephanie
Holman, Theodore R
et al.

Publication Date

2003-04-01

DOI

10.1021/bi020698o

Tryptophan 500 and Arginine 707 Define Product and Substrate Active Site Binding in Soybean Lipoxygenase-1

Viola C. Ruddat[&], Rakesh Mogul[&], Ilya Chorny[#], Cameron Chen[&], Noah Perrin[&], Stephanie Whitman[&], Victor Kenyon[&], Matthew P. Jacobson[#], Claude F. Bernasconi[&] and Theodore R. Holman[&*]

[&] Department of Chemistry and Biochemistry, University of California, Santa Cruz, CA, 95064, USA.

Department of Pharmaceutical Chemistry, University of California, San Francisco, CA 94143-2240, USA.

* To whom the correspondence should be sent.

Phone: (831) 459-5884

Fax: (831) 459-2935

E-mail: tholman@chemistry.ucsc.edu

Running title: Defining the soybean lipoxygenase binding site

This research has been supported NIH Grant GM56062-06 (TRH). Ilya Chorny is supported by a postdoctoral fellowship from the Alfred P. Sloan foundation and the U.S. Department of Energy.

RECEIVED DATE (to be automatically inserted after your manuscript is accepted if required according to the journal that you are submitting your paper to)

ABREVIATIONS

hLO, human lipoxygenase; methyl-end first, the insertion of the alkyl end of substrate/product into the pocket of the binding site first; carboxylate-end first", the insertion of the carboxylate end of the substrate/product into the pocket of the binding site first.sLO-1, soybean lipoxygenase-1; sLO-3, soybean lipoxygenase-3; WT, wild type soybean lipoxygenase; purple lipoxygenase, the HPOD bound Fe^{III} enzyme; Fe^{II}•HPOD, the complex of Fe^{II} and HPOD; Trp500Phe, the mutation of Trp500 to phenylalanine; Trp500Leu, the mutation of Trp500 to leucine; Arg707Leu, the mutation of Arg707 to leucine; Lys260Leu, the mutation of Lys260 to leucine; LA, linoleic acid; AA, arachidonic acid; HPOD, 13-(S)-hydroperoxy-9,11-(Z,E)-octadecadienoic acid (the oxidation product of LA); LA-D31, fully deuterated LA; 15-(S)-HPETE, 15-(S)-hydroperoxyeicosatetraeonic acid (the oxidation product of AA); K_D, dissociation constant of the enzyme/P complex; k_2, rate constant of peroxide scission; k_{obsd}, the observed pseudo-first-order rate constant; k_{cat}, the rate constant for product release; k_{cat}/K_m, the rate constant for substrate capture; KIE, primary kinetic isotope effect; k^H_{cat}/k^D_{cat}, the KIE for k_{cat}; $(k^H_{cat}/K_m)/(k^D_{cat}/K_m)$, KIE for k_{cat}/K_m;

ABSTRACT

There is much debate whether the fatty acid substrate of lipoxygenase binds "carboxylate-end first" or "methyl-end first" in the active site of soybean lipoxygenase-1 (sLO-1). In order to address this issue, we investigated the sLO-1 mutants, Trp500Leu, Trp500Phe, Lys260Leu and Arg707Leu with steady-state and stopped-flow kinetics. Our data indicate that the substrates (linoleic acid (LA), arachidonic acid (AA)), and the products (13-(S)-hydroperoxy-9,11-(Z,E)-octadecadienoic acid (HPOD) and 15-(S)-hydroperoxyeicosatetra-eonic acid (15-(S)-HPETE)) interact with the aromatic residue Trp500 (possibly π-π-interaction) and with the positively charged amino acid residue Arg707 (charge-charge-interaction). Residue Lys260 of soybean lipoxygenase-1 had little effect on either the activation or steady-state kinetics, indicating that both the substrates and products bind "carboxylate-end first" with sLO-1 and not "methyl-end first" as has been proposed for human 15-lipoxygenase.

Lipoxygenases (LO) catalyze the peroxidation of diene-containing fatty acids and belong to a class of non-heme iron metalloenzymes found in both plants and mammals (*1-3*). Mammalian lipoxygenases serve vital roles in the biosynthesis of lipoxins and leukotrienes, which are critical signaling molecules (*4, 5*). There are three major mammalian isozymes, 5-LO, 12-LO, and 15-LO, which oxygenate arachidonic acid (AA) at specific carbon centers (C5, C12 and C15, respectively) (*6*). These isozymes of human lipoxygenase have been shown to be involved in several human diseases: asthma (*7*) and prostate cancer (*8*) for human 5-LO (5-hLO), immune disorders (*9*) and breast cancer (*10, 11*) for human 12-LO (12-hLO) and atherosclerosis (*12*) and colorectal cancer (*13*) for human 15-LO (15-hLO).

In order to develop effective therapeutic agents against these diseases, an intimate knowledge of their active sites is needed so that specific inhibitors of a particular lipoxygenase isozyme can be designed. Sloane and coworkers made significant progress in this regard when they converted reticulocyte 15-hLO-1 into a "12-hLO" by increasing the active site volume; they proposed that the substrate sat deeper in the active site, with the hydrophobic methyl end inserted first[1] (*14*). This hypothesis was supported by site directed mutagenesis investigations of Gan et al., which suggested that Phe414 of 15-hLO-1 π-π-stacked with the C11-C12 double bond of the substrate and that the positively charged residue Arg402 interacted with the negatively charged carboxylate of the substrate (*15*). Because Arg402 is located close to the surface of 15-hLO-1, this study supported a "methyl-end first" binding of the substrate. In addition, mutagenesis experiments on Phe353 and Ile593 of rabbit 15-LO (15-rLO) also supported the

hypothesis that the size and shape of the active site defined the specificity and were consistent with a "methyl-end first" binding for mammalian 15-LO (*16, 17*).

Nevertheless, when the rabbit 15-LO (15-rLO) structure was compared with soybean lipoxygenase-1 (sLO-1), a debate concerning the manner in which the substrate bound to the active site developed. Amzel and coworkers proposed that, in order to obtain the known stereochemistry of the product, only a "carboxylate-end first" insertion of linoleic acid (LA) into the active site was plausible for sLO-1 (Figure 1a) and not a "methyl-end first" binding (Figure 1b) (*18*). However, Browner and coworkers suggested that the energy penalty for burying a charged residue into the hydrophobic cavity was too high for the Amzel model to be feasible (Figure 1a) (*19*). Their "methyl-end first" model argued that the observed differences in regio-selectivity primarily depended on the depth and size of the active site cavity.

Recently, the crystal structure of the ferric form of sLO-3 complexed with 13-hydroperoxy-9,11-(Z,E)-octadecadienoic acid (HPOD) (purple lipoxygenase) was determined, which supported the Amzel model ("carboxylate-end first" insertion) (*20*). The HPOD carboxylate was shown to interact with Arg726 (Arg707 in sLO-1) via a salt bridge and π-π-stacked with Trp519 (Trp500 in sLO-1) confirming that, for HPOD, burying the charge is not too much of an energy penalty to preclude binding. Nevertheless, it remained unclear if this binding mode was also utilized by the substrate. Kühn and coworkers investigated this issue with an elegant set of substrate modification experiments for sLO-1. Specifically, they found that if the substrate carboxylate was methylated and the C20 of AA was converted to an alcohol, oxygenation products at C5 were detected. These results are consistent with an inversion of the modified substrate

binding in the active site of sLO-1, relative to the normal binding of AA. However, the result did not address the question of what the normal binding of AA was, “methyl-end first” as suggested in 15-hLO-1 (*15-17*) or “carboxylate-end first” as seen for HPOD binding to sLO-3 (*20*).

In our current paper, we have investigated this issue in more detail by mutating the sLO-1 active site residues, Trp500 (Trp519 in sLO-3) and Arg707 (Arg726 in sLO-3), and determining their activation and catalytic kinetics. Our results demonstrate that both Trp500 and Arg707 are critical to product and substrate binding in the active site, which indicates that the substrate binds “carboxylate-end first” for sLO-1, the opposite orientation to what has been proposed for 15-hLO-1.

MATERIALS AND METHODS

Materials. All reagents used were reagent grade or better and were used without further purification. sLO-1 and its mutants were expressed and purified as described previously (*21*). Iron content of sLO-1 was determined on a Finnegan inductively coupled plasma mass spectrometer (ICP–MS), using an internal Co^{3+} standard and external standardized Fe solution. All enzyme concentrations were standardized to Fe content since only iron loaded sLO-1 is active.

Mutagenesis. Site directed mutants of sLO-1 were prepared by the Kunkel method as described previously and sequenced through the mutation (*21*). Trp500 was changed to leucine (Trp500Leu) and phenylalanine (Trp500Phe), Lys260 was mutated to leucine (Lys260Leu) and Arg707 was mutated to leucine (Arg707Leu). The mutant plasmids were transformed into *Escherichia coli* BL21 (DE3), expressed, and purified as described previously (*21*). Enzyme activities were determined with LA, observing the appearance of HPOD at 234 nm (ε=25,000).

Fatty Acid Purification. LA was purchased from Aldrich Chemical Co. HPOD was produced by reaction of LA with sLO-1, quenched with glacial acetic acid to pH 3, and exhaustively extracted with CH_2Cl_2. HPOD, LA and per-deuterated LA (LA- D31) were purified by a Waters 625 HPLC with a C18 column, as previously reported (Higgins Analytical, 5 micron, 250 x 10 mm, isocratic mobile phase: 85% Methanol: 15% H_2O: 0.1% Acetic acid at 3 mL/min). LA-D31 and LA were detected by in–line UV absorption (210 nm) and had a retention time of approximately 30 minutes; HPOD was detected at 234 nm with a retention time of 15 minutes. Product fractions were collected, evaporated to dryness, re-dissolved in ethanol and stored at –20 ˚C.

Enzymatic Product analysis. 15-(S)-hydroperoxyeicosatetraeonic acid (15-(S)-HPETE) products were produced by reaction of AA with sLO-1 and Arg707Leu respectively. The reaction was quenched with glacial acetic acid to pH 3, and exhaustively extracted with ethyl acetate. 15-(S)-HPETE products were analyzed by a Waters 625 HPLC with a C18 column (Higgins Analytical, 5 micron, 250 x 10 mm, isocratic mobile phase: 75% Methanol: 25% H_2O: 0.1% Acetic acid at 1 mL/min) and were detected by in–line UV absorption (210 nm). Samples of 15-(S)-HPETE (from an AA/15-hLO reaction), 12-HPETE (from an AA/12-hLO reaction) and 5-HPETE (purchased from Cayman) were analyzed by the same HPLC method as standards.

Purification of LA-D31. A per-deuterated fatty acid mixture was purchased from Cambridge Isotope laboratories. The fatty acid mixture was separated using a modification of the protocol described by Holman et al (*22*). A column containing 100 g of Ag-silica and 100 mL of hexane was prepared. The fatty acid mixture was loaded and eluted with 200 mL of 2% ethyl acetate in hexane (two fractions), 400 mL of 5 % ethyl acetate in hexane (30 fractions), and 200 mL of 10% ethyl acetate in hexane. The pure LA-D31 was detected in fractions 17-25 of the 5% ethyl acetate in hexane. These fractions were combined, the solvent evaporated and de-esterified overnight in 10 mL of EtOH, 0.35 g of NaOH and 3.5 mL of water. The ensuing mixture was acidified (1.5 mL of glacial acetic acid and 65 mL of water added) and the LA-D31 extracted with three-5 mL portions of methylene chloride. After evaporation of the solvent, the purity of LA-D31 was verified with the Quattro II mass spectrometer by the absence proteo-LA and other fatty acid impurities, such as perdeutero-palmitic and perdeutero-oleic acid. To ensure that no singly-protonated substrate (LA-D30-H1, proton on C13) was present, the

purified LA-D31 was briefly reacted with lipoxygenases and re-purified to remove the LA-D30-H1 product.

Stopped-Flow Kinetics. Kinetic measurements of the enzyme activation were carried out under pseudo-first-order conditions (with the enzyme as the minor component) using a DX.17MV Applied Photophysics spectrofluorometer equipped with a 150-watt xenon arc lamp light source and 320 nm cut-off filter, as reported previously (*23*)**.** Oxidation of ferrous to ferric sLO-1 was followed by observing the temporal change in fluorescence emission above 320 nm (λ_{ex}= 280 nm). The kinetic measurements of the activation were carried out under pseudo-first-order conditions with the enzyme as the minor component. The concentrations of enzyme, HPOD and 15-(S)-HPETE were verified on an Agilent 8453 UV- visible spectrophotometer (λ_{max}= 234 nm for the hydroperoxy-product and λ_{max}= 280 nm for the enzyme). All fluorescence measurements were performed using ~ 2 μM enzyme (WT, Trp500Leu, Trp500Phe, or Lys260Leu) and over a range of 20 to 200 μM hydroperoxy-product in 0.1 M sodium borate buffer (pH 9.2) at 25˚C. For the determination of the kinetic parameters of activation for Arg707Leu, the range of hydroperoxy-product was increased up to 800 μM. In order to determine K_D and k_2, kinetic runs were performed at 10 or more different concentrations of the hydroperoxy-product; each pseudo-first-order rate constant (k_{obsd}) is the average of at least 5 determinations. The stopped-flow apparatus was rinsed with HNO_3, KOH and water after every couple of runs to prevent enzyme build up and thus artifacts in the kinetics.

Steady-State Kinetics. Lipoxygenase turnover rates were determined by following the formation of product at 234 nm (ε = 25,000 $M^{-1}cm^{-1}$) with a Hewlett–Packard 8453 or

Perkin Elmer Lambda 40 UV–vis spectrophotometer. Destruction of the hydroperoxy-product by the diode array spectrophotometer was negligible under these reaction conditions. All reaction solutions were 2 ml in volume, run at room temperature (23-25˚C), and constantly stirred with a rotating magnetic bar. For the reactions with LA and AA, kinetic runs were performed in 0.1 M borate (pH 9.2). Substrate solutions used in each experiment were measured for accurate LA and AA concentration by quantitatively converting substrate to product using WT sLO-1. Enzymatic rates were measured from 1 to 80 μM substrate concentration and reactions were initiated by the addition of enzyme to final concentrations of ≈ 3 nM for all mutants. All kinetic parameters were determined by non–linear regression using Kaleidagraph software (Abelbeck).

Determination of K_D for the Fe^{III}•HPOD Complex. To determine the K_D of purple sLO-1, Fe^{III} was titrated with increments of HPOD as described in Materials and Methods. The K_D determination was performed as previously described (*24, 25*). Increasing amounts of HPOD were added to enzyme at 4˚C in 0.1 M borate. The formation of the Fe^{III}•HPOD (purple lipoxygenase) was followed at 580 nm (ε = 1550 $M^{-1}cm^{-1}$for the WT and Trp500Phe and ε = 899 $M^{-1}cm^{-1}$for Trp500Leu) with a Perkin Elmer Lambda 40 UV–vis spectrophotometer. All reactions were carried out in 1.8 ml 100 mM borate, run at 4˚C, and constantly stirred with a rotating magnetic bar. All experiments were determined using 40 μM enzyme and a range of 40 to 400 μM hydroperoxy-product. The measurements were completed within 20 minutes and carried out in duplicate. Dissociation constants were determined by non–linear regression using Kaleidagraph software (Abelbeck).

Kinetic Isotope Effect. Steady-state kinetics were carried out as described previously (*22*). All reactions were carried out in 2 mL of 100 mM borate at pH 9.2. The initial rates were measured over a range of 3 to 60 μM LA for the protonated substrate and over a range of 3 to 80 μM LA for the deuterated substrate. Reactions were initiated with enzyme addition (~2-4 nM enzyme for the protonated substrate and ~0.2-0.4 μM for the deuterated substrate). Each time the conditions were optimized such that the maximum rate was ~0.01 abs/s^{-1}. The measured rates were fit to the Michaelis-Menten equation with Sigma Plot software.

RESULTS AND ANALYSIS

Protein Purification. WT, Trp500Leu, Trp500Phe, Lys260Leu and Arg707Leu were purified (greater than 90 % purity, as determined by SDS-PAGE), with protein expression yields of ~ 8-20 mg/L of culture and contained 89%, 76%, 86%, 59%, and 22% Fe, respectively (error for each metal determination is approximately 5%).

Determination of activation kinetics. The activation of sLO-1 can be described by Equation 1, where HOOR stands for hydroperoxy-product (HPOD or 15-(S)-HPETE).

$$Fe^{2+} + HOOR \underset{k_{-1}}{\overset{k_1}{\rightleftharpoons}} Fe^{2+}\bullet HOOR \xrightarrow{k_2} Fe^{3+}(OH) + \text{unknown} \qquad (1)$$

In the analysis to follow we used K_D, as previously defined: $K_D = K_m$ since $\frac{k_{-1} + k_2}{k_1} = K_m$ and $k_{-1} >> k_2$, (*26, 27*). We will use K_D from here on. Rates of the formation of the oxidized ferric enzyme ($Fe^{III}(OH)$) were measured by monitoring the change in fluorescence of the enzyme above 320 nm. Pseudo first order rate constants were determined with increasing product concentration (HPOD or 15-(S)-HPETE) with WT and all mutants. Figure 2 shows a plot of k_{obsd} vs. [HPOD] with WT and all four mutants; it represents a saturation curve consistent with an accumulation of Fe^{III}•HPOD at high concentrations.

The expression for k_{obsd} is given in Equation 2 (P represents the hydroperoxy-product).

$$k_{obsd} = \frac{k_2[P]}{K_D + [P]} \qquad (2)$$

Using non-linear regression methods, the dissociation constant, K_D, and the rate constant for the rate determining second step, k_2, were determined for WT, Trp500Leu, Trp500Phe, Lys260Leu, and Arg707Leu with HPOD and 15-(S)-HPETE (Table 1a) (*23*).

HPOD bound to the WT with a K_D of 26 ± 0.8 μM and oxidized the iron center with a k_2 of 180 ± 6 s^{-1} (*23*)**.** Trp500Leu yielded increases in K_D to 81 ± 12 μM and k_2 to 542 ± 36 s^{-1} (Table 1a). This loss of aromaticity and steric bulk at residue 500 (Trp500Leu), resulted in a ~3-fold decrease in the strength of product binding and a 3-fold increase in the magnitude of k_2. Reintroduction of aromaticity at residue 500, Trp500Phe, yielded a K_D of 34 ± 8 μM and a k_2 of 387 ± 30 s^{-1}, which is comparable to the values for WT sLO-1; however, k_2 is 2-fold greater than for WT.

The activation kinetics for WT with 15-(S)-HPETE were markedly different than those with HPOD. The K_D for the activation of the WT with 15-(S)-HPETE was 49 ± 5 μM and the rate constant for the second step, k_2 was 402 ± 17 s^{-1} (Table 1a); both are approximately 2-fold greater than the values for WT with HPOD. Interestingly, mutations of Trp500 affected the activation kinetics of 15-(S)-HPETE less than that of HPOD. Trp500Leu had a K_D of 46 ± 10 μM and a k_2 of 318 ± 32 s^{-1}, while Trp500Phe led to a K_D of 44 ± 5 μM and a k_2 of 391 ± 18 s^{-1}.

The mutation of residue Lys260 to a leucine (Lys260Leu) had almost no effect on the activation kinetics for either HPOD or 15-(S)-HPETE (Table 1a). However, the mutation of Arg707 to leucine (Arg707Leu) led to dramatic changes in its activation kinetics, especially on product binding. The K_D for the activation of Arg707Leu with HPOD was 189 ± 17 μM (7-fold greater than WT) and k_2 was 34.5 ± 5.5 s-1 (5-fold slower than WT) (Table 1a). Activation of Arg707Leu with 15-(S)-HPETE led to a K_D of 491 ± 112 μM (7-fold greater than WT) and a k_2 of 69 ± 8 s^{-1} (3-fold slower than WT).

Determination of K_D for the Fe^{III}•HPOD Complex. Titration of Fe^{III}-sLO-1 with HPOD produces an Fe^{III}•HPOD complex (purple lipoxygenase) which has a λ_{max} at 580

nm due to the ligand-to-metal charge transfer band of HPOD bound to the ferric form of sLO-1 (Scheme 1). The half-life for Fe^{III}•HPOD was approximately 30 minutes at 25 ˚C (*27*); however, at 4 ˚C no decay was observed after 30 minutes. The K_D for the formation of purple lipoxygenase was determined by the addition of HPOD to Fe^{III}-sLO-1 under steady-state conditions with WT, Trp500Phe, Trp500Leu, Arg707Leu, and Lys260Leu (Table 1b) (*25*). The K_D was determined to be 31.3 ± 3.6 μM for the WT, 87.2 ± 2.3 μM for Trp500Leu, 49.8 ± 1.9 μM for Trp500Phe, 39.1 ± 5.8 μM for Lys260Leu, and 160 ± 15 μM for Arg707Leu. These values correspond in trend and magnitude remarkably well to those of the K_D of the activation, with the greatest increases in K_D for Trp500Leu and Arg707Leu. We were not able to determine the K_D for 15-(S)-HPETE bound to sLO-1, because the half-life of the complex at 4 ˚C was too short.

Steady-State Kinetics. The steady-state parameters of k_{cat} and k_{cat}/K_m ($K_m \neq K_D$, in contrast to activation kinetics) were determined for all enzymes using LA and AA (Table 2). Comparison of the kinetic values for LA catalysis between the mutants demonstrated comparable trends as those for HPOD activation. Trp500Leu displayed decreases in both k_{cat} (132+/-3 s^{-1}) and k_{cat}/K_m (16+/-3.2 $s^{-1}M^{-1}$). The kinetic parameters were partially restored with the Trp500Phe mutant which manifested a k_{cat} of 249+/-19 s^{-1} and a k_{cat}/K_m of 24.2+/-2.8 $s^{-1}M^{-1}$. The mutation of Lys260Leu did not lead to significant changes in k_{cat} or k_{cat}/K_m; however, Arg707Leu displayed decreases in both k_{cat} (174 ± 11 s^{-1}), and k_{cat}/K_m (8.9+/- 1.3 $s^{-1}M^{-1}$), both approximately 2-fold lower than WT.

With AA as the substrate, k_{cat} and k_{cat}/K_m increased dramatically for WT and all mutants, relative to the LA values, however, their trends were comparable to those seen

for LA (Table 2). Trp500Leu demonstrated a k_{cat}/K_m comparable to WT (41.0+/- 7.1 $s^{-1}M^{-1}$), but its k_{cat} decreased by approximately 50 % (221± 10 s^{-1}). Trp500Phe regained WT activity with a k_{cat} of 495+/-10 s^{-1} and a k_{cat}/K_m of 43.5+/-2.8 $s^{-1}M^{-1}$. Lys260Leu manifested a comparable k_{cat} to WT (454+/-22 s^{-1}) but a depressed k_{cat}/K_m (26.1+/- 3 $s^{-1}M^{-1}$). Arg707Leu displayed a more dramatic decrease in both k_{cat} (370+/-5 s^{-1}) and k_{cat}/K_m (18.5+/-2 $s^{-1}M^{-1}$), relative to Lys260Leu, as seen previously with LA as the substrate.

Enzymatic Product analysis. At a solvent ratio of 75% Methanol: 25% H_2O : 0.1% Acetic acid, the retention time of 5-HPETE was observed to be 18 minutes, 15-(S)-HPETE to be 20.5 minutes and 12-HPETE to be 23 minutes. The turnover product of WT sLO-1 and Arg707Leu were then compared to these standards and determined to be 100% 15-(S)-HPETE without a trace of either 12-HPETE or 5-HPETE, indicating no substrate inversion.

Kinetic Isotope Effects. The primary kinetic isotope effect (C13 deuterated on LA) for catalysis (k_{cat}^H/k_{cat}^D) was determined for WT, Trp500Leu, and Trp500Phe. Our WT results are in agreement with previous results in that there was no temperature dependence in k_{cat}^H/k_{cat}^D (k_{cat}^H/k_{cat}^D = 64 ± 2 at 20° and 62 ± 4 at 30°C) (*28*). The values for k_{cat}^H/k_{cat}^D also remained constant at the two temperatures for Trp500Phe and Trp500Leu, although their magnitudes were higher than WT. They were determined to be 87 ± 8 (20°C) and 82 ± 4 (30°C) for Trp500Phe and 78 ± 3 (20°C) and 80 ± 3 (30°C) for Trp500Leu. The k_{cat}/K_m KIE increased with temperature for WT (40 ± 5 (20°C) and 56 ± 10 (30°C)), as previously reported (*29, 30*). The k_{cat}/K_m KIE for Trp500Leu also increased with temperature (85 ± 12 (20°C) and 119 ± 19 (30°C)), however, the k_{cat}/K_m

KIE for Trp500Phe, did not change significantly with temperature (72 ± 20 (20°C) and 77 ± 12 (30°C)).

Computational Docking. Glide (FirstDiscovery Software Suite, Schrodinger Inc) (*31, 32*) was used for flexible docking. Glide uses an expanded version of the ChemScore empirical scoring function (*33, 34*), which is designed to reproduce binding free energies of a diverse set of protein-ligand complexes. The Glide docking algorithm has recently been shown to outperform other docking algorithms in its ability to reproduce co-crystallized poses from a set of 69 ligand-receptor complexes from the PDB (*35*).

The apo-sLO-1 (1f8n) receptor was prepared using standard procedures, i.e., by adding hydrogens to the crystal structure and specifying the correct charge and atom type for the metal ion. The binding pocket was identified by structurally aligning 1f8n to the holo sLO-3 (1ik3) crystal structure with HPOD bound (*20*) using the Combinatorial Extension algorithm (CE) (*36*). Following the alignment, the coordinates of the HPOD bound to 1ik3 were transferred to 1f8n and used to define the active site. The *impref* utility script was then used to energy minimize residues surrounding the ligand, subject to the restriction that heavy atoms move no more than 0.3 Å RMSD. Mutants were prepared by modifying the relevant residues followed by minimization as described above. After completing the receptor preparation step, HPOD, 15-(S)-HPETE, LA, and AA, were docked using the "extra precision" Glide algorithm.

The Glide scoring function is optimized to predict hydrogen bonding, charge-charge, and lipophilic type interactions, but it does not contain any terms that explicitly model π-π-stacking. For this reason we have only modeled HPOD, 15-(S)-HPETE, LA and AA in WT sLO-1 and its mutant Arg707Leu. The data presented in Table 3 indicate that

replacement of Arg707 with leucine lowers the Glide score for both products and both substrates, with 15-(S)-HPETE demonstrating the largest decrease in binding interaction upon replacement of Arg707 with a leucine.

DISCUSSION

There has been significant discussion in the literature regarding the mode of substrate binding for both sLO-1 and 15-hLO-1 and whether the polar carboxylate of the substrate is buried deep in the active site or not (*15, 18, 19*). The issue is complicated by the fact that there is no clear entrance to the active site for any of the lipoxygenase crystal structures (*20, 37, 38*). Mutagenesis and crystallographic data, for 15-hLO-1 and 15-rLO, suggest that the fatty acid substrate enters into the active site "methyl-end first" (*37*) but crystallographic data for sLO-3 indicates that the product enters into the active site "carboxylate-end first" (*20*)**.** In the current paper, we have mutated two residues, Trp500 and Arg707, in the active site of sLO-1 in order to determine the factors determining the binding of both substrate and product in the active site of sLO-1.

The activation kinetics of WT sLO-1 (K_D = 26 ± 0.6 μM and k_2 = 180 ± 6 s^{-1}), reported previously by Ruddat et al., clearly demonstrate that the product binds tightly to the ferrous species of sLO-1 to form a Fe^{II}•HPOD complex (*23*). The mutation of Trp500 to a non-aromatic leucine, however, causes a 3-fold increase in the K_D compared to WT, whereas the Trp500Phe mutation manifests only a small change in its K_D value (Table 1a). This result clearly indicates that an aromatic residue at position 500 increases product affinity, suggesting π-π-interaction for sLO-1, as previously demonstrated for catalysis by mutagenesis studies of 15-hLO-1 (*15*).

The K_D values of product bound to the ferric form of Trp500Leu and Trp500Phe (Fe^{III}•HPOD or purple lipoxygenase) (Table 1a and Table 1b) were within error of the K_D values of the Fe^{II}•HPOD complex, with the K_D for Trp500Leu increasing 3-fold but

Trp500Phe only increasing slightly compared to WT. These data indicate that the π-π-interaction between Trp500 and HPOD occurs in both the ferrous and ferric forms of sLO-1 and that the oxidation state change does not disrupt this interaction. These K_D data are consistent with crystallography data which indicated only minor structural variation between the ferrous crystal structure of sLO-3 and the Fe^{III}•HPOD sLO-3 structure, with a root mean deviation of 0.4 Å between the two forms (*20*).

Interestingly, the K_D values for Fe^{II}•15-(S)-HPETE, the product of the un-natural substrate AA, were dramatically different than those of Fe^{II}•HPOD complex. The WT K_D for 15-(S)-HPETE was almost twice that of the WT K_D value for HPOD, which indicates that 15-(S)-HPETE binds less tightly to the active site of sLO-1 than HPOD. In addition, the K_D for 15-(S)-HPETE did not change with loss of the aromatic Trp500 (K_D (WT) = 49.0 ± 5 μM and K_D (Trp500Leu) = 46.3 ± 10.3 μM), indicating that 15-(S)-HPETE does not π-π-stack with Trp500, contrary to that seen for HPOD. These data suggest a different binding mode in the sLO-1 active site between HPOD and 15-(S)-HPETE with respect to Trp500.

Another important interaction previously seen for 15-hLO-1 was the charge-charge-interaction between the positively charged active site residue Arg402 and the negatively charged carboxylate of the substrate (*15*). Gan et al. found that removal of the cationic Arg402 resulted in a decrease in k_{cat}/K_m for 15-hLO-1 but k_{cat} did not change. This result coupled with the structure determination of the homologous lipoxygenase, 15-rLO, suggested that for mammalian 15-LO, the substrate binds “methyl-end first” (Figure 1b). If sLO-1 binds its substrate in a similar manner, then Lys260 would be predicted to form a charge-charge-interaction. Amzel and coworkers disagreed with this

assessment of substrate binding in sLO-1 and proposed Arg707 as the residue for charge-charge-interaction (*38*). This hypothesis had the substrate entering "carboxylate-end first", opposite to the mammalian 15-LO model (Figure 1a). We therefore tested these two possible charge-charge-interactions by mutating the active site residues Lys260 and Arg707 in sLO-1, but found that only the Arg707 mutation manifested any effect on activation and catalysis. The K_D for activation of Arg707Leu (Fe^{II}•HPOD) increased dramatically to 189 μM, while the K_D for Lys260 did not change, indicating that Arg707 interacts with the carboxylic acid of HPOD. Arg707Leu also demonstrated an increased K_D (160 μM) for HPOD bound to the ferric species, comparable to that found for the ferrous form. These results are consistent with the Fe^{III}•HPOD crystal structure of sLO-3, which showed a clear interaction between the carboxylate of HPOD and Arg729 (the Arg707 homologue in sLO-1) (*20*) and confirm the "carboxylate-end first" binding model for sLO-1. Interestingly, the increase in K_D for the Fe^{II}•HPOD species of Arg707Leu is more than twice as large as that observed for Trp500Leu, indicating a more significant energy contribution for charge-charge-interactions than π-π-stacking.

The K_D for 15-(S)-HPETE binding to Arg707Leu also demonstrated a significant increase relative to WT, indicating an important charge-charge-interaction, like that with HPOD. This similarity between HPOD and 15-(S)-HPETE binding is in contrast to the dissimilar results found for both product interactions with Trp500. This difference can be rationalized by the fact that 15-(S)-HPETE has two additional double bonds and is two carbons longer than HPOD, which extends the substrate double bond past the Trp500 position and potentially removes the π-π-stacking (Figure 3).

In order to probe further the differences in binding between HPOD and 15-(S)-HPETE, we modeled them both into the active site of WT sLO-1 and Arg707Leu, utilizing the docking program Glide. The resultant Glide scores help rationalize the K_D data (Table 3). For both HPOD and 15-(S)-HPETE, the mutation of Arg707Leu decreased the Glide score by 40 and 43%, respectively, indicating the importance of Arg707 in stabilizing the carboxylate of both HPOD and 15-(S)-HPETE, as shown in Figure 3. With regard to π-π-stacking, we reiterate that the Glide scoring function does not explicitly model this type of interaction. Nonetheless, we do observe that Trp500 is in closer proximity to the double bond closest to the peroxide in HPOD than in 15-(S)-HPETE (3.95 Å vs. 4.94 Å), as shown in Figure 3. This change in interaction distance helps to rationalize the difference in binding affinity of HPOD and 15-S-HPETE to Trp500Leu.

Steady-state kinetics experiments were performed to determine if similar binding interactions between Arg707 and Trp500 with the products could also be observed for substrate catalysis. For LA, the mutants displayed comparable trends in kinetic parameter changes as that with the HPOD dissociation constants. The k_{cat} (product release) and k_{cat}/K_m (substrate capture) for Trp500Leu both decreased relative to WT, with a greater effect on product release. However, if an aromatic residue replaces Trp500 (Trp500Phe), the k_{cat} and k_{cat}/K_m are comparable to the kinetic values of WT. This data indicates that, for catalysis, both the rate of the substrate capture and the rate of product release for LA are dependent on Trp500, implying that π-π-stacking is involved in both kinetic processes. The mutant Arg707Leu also manifested lower k_{cat} and k_{cat}/K_m values than WT, with a greater effect on substrate capture. Lys260Leu,

however, manifested no change in kinetic parameters, which indicates that LA interacts with Arg707 and binds to sLO-1 “carboxylate-end first”.

The kinetics for AA with the sLO-1 mutants manifested similar trends as those for LA. Trp500Leu displayed a marked decrease in its k_{cat}, while Trp500Phe manifests little change in kinetic parameters, relative to WT. This result is consistent with a π-π-interaction between Trp500 and AA, similar to that seen for LA. It is interesting to note that, for both LA and AA, k_{cat} is affected more than k_{cat}/K_m, indicating that π-π-interactions with Trp500 are more critical for the rate of product release than substrate capture. This is in contrast to the K_D value for 15-(S)-HPETE binding to the ferrous form of sLO-1, which clearly shows that Trp500 does not interact with 15-(S)-HPETE, suggesting a greater interaction between AA and Trp500 than between 15-(S)-HPETE and Trp500.

Arg707Leu also manifested significant changes in kinetic parameters with AA as the substrate, with a decrease in both k_{cat} and k_{cat}/K_m, indicative of a “carboxylate-end first” binding for AA, like LA. Also similar to that seen for LA, the k_{cat}/K_m for Arg707Leu is more greatly affected than k_{cat}, implying a greater role for Arg707 in substrate capture than product release, opposite to that observed for the role of Trp500.

The interaction of LA and AA were subsequently modeled into the active site of sLO-1 with the docking program Glide, and the binding poses determined for LA and AA indicated a significant interaction with Arg707 (results not shown), consistent with experimental results. In addition, the poses displayed the appropriate positioning for hydrogen atom abstraction (C11 for LA and C13 for AA), which indicates that there is sufficient volume in the active site to accommodate the longer AA substrate as well as

the shorter LA and still have them both interact with Arg707 via a "carboxylate-end first" binding. Nevertheless, it should be noted that the degrees of freedom for substrate docking are much greater than that for product binding, so the details of the substrate docking data are less reliable.

The KIE of k_{cat} for LA were determined for both Trp500Leu and Trp500Phe to be large and temperature independent. This is consistent with the previous results on WT sLO-1 and indicates that the rate of product release for both of these mutants is solely limited by hydrogen atom abstraction (*39-41*). The temperature dependence of the k_{cat}/K_m KIE for WT is due to competing rate-limiting steps (viscosity, hydrogen bond rearrangement and hydrogen atom abstraction) (*21, 42*). Trp500Leu manifested a large KIE and temperature dependence, indicating that there are multiple rate limiting steps involved in substrate capture, similar to that seen in WT. Trp500Phe also had a large KIE but limited temperature dependence, indicating that hydrogen abstraction is the principal rate limiting step. This variation in the degree of temperature dependence has been previously observed with other mutations of sLO-1 (*30, 41*).

The activation kinetics (Equation 1) are fit with a two step kinetic model consisting of an equilibrium step (K_D) and an irreversible step (k_2); K_D represents the formation of the hydroperoxy-product/enzyme complex and k_2 represents the rate of ferrous-peroxide bond scission. The magnitudes of the k_2 values for the mutants are difficult to interpret. For both Trp500Leu and Trp500Phe, the k_2 values increase dramatically relative to WT (300% and 220%, respectively). A possible explanation for this is that the Fe^{II}•HPOD complex is destabilized by the removal of tryptophan (greater K_D values), while the energy of the transition state complex remains the same, effectively reducing the

activation energy and increasing the rate of k_2 (Figure 4a). However, this explanation is inconsistent with the results for Arg707Leu. The k_2 for Arg707Leu decreases relative to WT, even though its K_D has increased by a larger factor than the K_D of Trp500Leu (indicating an even more destabilized enzyme/HPOD complex). This implies that for Arg707Leu, the energy of the transition state complex has increased more than that of the Fe^{II}•HPOD complex, effectively increasing the activation energy and lowering the rate of k_2 (Figure 4b). This supports our hypothesis that arginine plays a greater role in the activation than tryptophan. Additional experiments are currently in progress to help clarify these reaction profile differences between the two mutants.

Conclusions. Our results clearly establish that both π-π-interactions with Trp500 and charge-charge-interactions with Arg707 are involved in the recognition of substrates and hydroperoxy-products. These data also indicate that AA, the non-natural substrate of sLO-1, and its product, 15-(S)-HPETE, both interact with Arg707 but have subtle binding differences that could account for the catalytic turnover differences between LA and AA. Finally, the results of our investigations support the hypothesis that for sLO-1, both the substrate and the product bind "carboxylate-end first" in the active site and that charge-charge-interactions are a greater factor in their binding energies than π-π-interactions.

ACKNOWLEDGEMENTS

This paper is dedicated to C. T. Walsh in recognition of his 60th birthday.

REFERENCES

1. Gardner, H. W. Recent investigations into the lipoxygenase pathway of plants (1991) *Biochim. Biophys. Acta 1084*, 221-239.

2. Siedow, J. N. Plant lipoxygenase : structure and function (1991) *Annu. Rev. Plant Physiol. Plant Mol. Biol 42*, 145-188.

3. Veldink, G. A., and Vliegenthart, J. F. G. Lipoxygenases, nonheme iron-containing enzymes (1984) *Adv. Inorg. Biochem. 6*, 139-161.

4. Samuelsson, B., Dahlen, S. E., Lindgren, J. A., Rouzer, C. A., and Serhan, C. N. Leukotrienes and lipoxins: structures, biosynthesis, and biological effects (1987) *Science 237*, 1171-1176.

5. Ford-Hutchinson, A. W., Gresser, M., and Young, R. N. 5-Lipoxygenase (1994) *Annu. Rev. Biochem 63*, 383-417.

6. Brash, A. R. Lipoxygenases: occurrence, functions, catalysis, and acquisition of substrate (1999) *Journal of Biological Chemistry 274*, 23679-23682.

7. Nakano, H., Inoue, T., Kawasaki, N., Miyataka, H., Matsumoto, H., Taguchi, T., Inagaki, N., Nagai, H., and Satoh, T. Synthesis and biological activities of novel antiallergic agents with 5-lipoxygenase inhibiting action (2000) *Bioorganic and Medicinal Chemistry 8*, 373-380.

8. Gosh, J., and Myers, C. E. Inhibition of arachidonate 5-lipoxygenase triggers massive apoptosis in human prostate cancer cells (1998) *Proc. Natl. Acad. Sci. 95*, 13182-13187.

9. Hussain, H., Shornick, L. P., Shannon, V. R., Wilson, J. D., Funk, C. D., Pentland, A. P., and Holtzman, M. J. Epidermis contains platlet-type 12-lipoxygenase that is overexpressed in germinal layer keratinocytes in psoriasis (1994) *Am. J. Physiol. 266*, C243-C253.

10. Connolly, J. M., and Rose, D. P. Enhanced angiogenesis and growth of 12-lipoxygenase gene-transfected MCF-7 human breast cancer cells in athymic nude mice (1998) *Cancer Letters 132*, 107-112.

11. Natarajan, R., and Nadler, J. Role of lipoxygenases in breast cancer. (1998) *Front. Biosci. 3*, E81-E88.

12. Harats, D., Shaish, A., George, J., Mulkins, M., Kurihara, H., Levkovitz, H., and Sigal, E. Overexpression of 15-lipoxygenase in vascular endothelium accelerates early atherosclerosis in LDL receptor-deficient mice (2000) *Arteriosclerosis Thrombosis and Vascular Biology 20*, 2100-2105.

13. Kamitani, H., Geller, M., and Eling, T. Expression of 15-lipoxygenase by human colorectal carcinoma Caco-2 cells during apoptosis and cell differentiation (1998) *J. Biol. Chem. 273*, 21569-21577.

14. Sloane, D., Leung, R., Craik, C., and Sigal, E. A primary determinant for lipoxygenase positional specificity (1991) *Nature 354*, 149-152.

15. Gan, Q.-F., Browner, M. F., Sloane, D. L., and Sigal, E. Defining the arachidonic acid binding site of human 15-lipoxygenase. Molecular modeling and mutagenesis (1996) *J. Biol. Chem. 271*, 25412 - 25418.

16. Borngräber, S., Browner, M., Gillmor, S., Gerth, C., Anton, M., Fletterick, R., and Kühn, H. Shape and specificity in mammalian 15-lipoxygenase active site. The functional interplay of sequence determinants for the reaction specificity (1999) *J. Biol. Chem. 274*, 37345-37350.

17. Borngräber, S., Kuban, R. J. and Kühn, A. N. Phenylanaline is a primary determinant for the positional specificity of mammalian 15-lipoxygenases (1996) *J. Mol. Biol. 264*, 1145-1153.

18. Prigge, S. T., Gaffney, B. J., and Amzel, L. M. Relation between positional specificity and chirality in mammalian lipoxygenases (1998) *Nature Structural Biology 5*, 178-179.

19. Browner, M., Gillmor, S.A. and Fletterick, R. Burying a charge (1998) *Nature Structural Biology 5*, 179.

20. Skrzypczak-Jankun, E., Bross, R., Carroll, R., Dunham, W., Funk, M. Three-dimensional structure of a purple lipoxygenase (2001) *J. Am. Chem. Soc. 123*, 10814-10820.

21. Holman, T. R., Zhou, J., and Solomon, E. I. Spectroscopic and functional characterization of a ligand coordination mutant of soybean lipoxygenase-1: first coordination sphere analogue of human 15-lipoxygenase (1998) *J. Am. Chem. Soc. 120*, 12564-12572.

22. Mogul, R., Johansen, E., and Holman, T. Oleyl sulfate reveals allosteric inhibition of soybean lipoxygenase-1 and human 15-lipoxygenase (2000) *Biochemistry 39*, 4801-4807.

23. Ruddat, V. C., Whitman, S., Holman, T. R., and Bernasconi, C. F. Stopped-flow kinetic investigations of the activation of soybean lipoxygenase-1 and the influence of inhibitors on the allosteric site (2003) *Biochemistry 42*, 4172-4178.

24. Wang, Z. X., Killilea, S. D., and Srivastava, D. K. Kinetic evaluation of substrate-dependent origin of the lag phase in soybean lipoxygenase-1 catalyzed reactions (1993) *Biochemistry 32*, 1500-1509.

25. Wang, Z.-X.A Simple method for determining kinetic constants of slow, tight-binding inhibition (1993) *Anal. Biochem. 213*, 370-377.

26. Verhagen, J., Veldink, G. A., Egmond, M. R., Vliegenthart, J. F., Boldingh, J., and van der Star, J. Steady-state kinetics of the anaerobic reaction of soybean lipoxygenase-1 with linoleic acid and 13-L-hydroperoxylinoleic acid (1978) *Biochim Biophys Acta 529*, 369-379.

27. Egmond, M. R., Fasella, P. M., Veldink, G. A., Vliegenthart, J. F., and Boldingh, J. On the mechanism of action of soybean lipoxygenase-1. A stopped-flow kinetic

study of the formation and conversion of yellow and purple enzyme species (1977) *Eur J Biochem 76*, 469-479.

28. Rickert, K. W., and Klinman, J. P. Nature of hydrogen transfer in soybean lipoxygenase 1: separation of primary and secondary isotope effects (1999) *Biochemistry 38*, 12218-12228.

29. Tomchick, D. R., Phan, P., Cymborowski, M., Minor, W., and Holman, T. R. Structural and functional characterization of second-coordination sphere mutants of soybean lipoxygenase-1 (2001) *Biochemistry 40*, 7509-7517.

30. Knapp, M., Rickert, K. and Klinman, J. Temperature-dependent isotope effects in soybean lipoxygenase-1: correlating hydrogen tunneling with protein dynamics (2002) *J. Am. Chem. Soc 124*, 3865-3874.

31. Halgren, T. A., Murphy, R. B., Friesner, R. A., Beard, H. S., Frye, L. L., Pollard, W. T., and Banks, J. L. Glide: a new approach for rapid, accurate docking and scoring. 2. Enrichment factors in database screening (2004) *J Med Chem 47*, 1750-1759.

32. Friesner, R. A., Banks, J. L., Murphy, R. B., Halgren, T. A., Klicic, J. J., Mainz, D. T., Repasky, M. P., Knoll, E. H., Shelley, M., Perry, J. K., Shaw, D. E., Francis, P., and Shenkin, P. S. Glide: a new approach for rapid, accurate docking and scoring. 1. Method and assessment of docking accuracy (2004) *J Med Chem 47*, 1739-1749.

33. Eldridge, M. D., Murray, C. W., Auton, T. R., Paolini, G. V., and Mee, R. P. Empirical scoring functions: The development of a fast empirical scoring function to estimate the binding affinity of ligands in receptor complexes (1997) *J. Com. Aided Mol. Des. 11*, 425-445.

34. Eldridge, M. D., Vervoort, H. C., Lee, C. M., Cremin, P. A., Williams, C. T., Hart, S. M., Goering, M. G., O'Neil-Johnson, M., and Zeng, L. High-throughput method for the production and analysis of large natural product libraries for drug discovery (2002) *Anal. Chem. 74*, 3963-3971.

35. LKontoyianni, M., McClellan, L. M., and Sokol, G. S. Evaluation of docking performance: comparative data on docking algorithms (2004) *J. Med. Chem. 47*, 558-565.

36. Shindyalov I.N. and Bourne, P. E. Protein structure alignment by incremental combinatorial extension (CE) of the optimal path (1998) *Protein Engineering 11*, 739-747.

37. Gillmor, S. A., Villasenor, A., Fletterick, R., Sigal, E., and Browner, M. The structure of mammalian 15-lipoxygenase reveals similarity to the lipases and the determinants of substrate specificity (1997) *Nature Structural Biology 4*, 1003-1009.

38. Boyington, J. C., Gaffney, B. J., and Amzel, L. M. The three-dimensional structure of an arachidonic acid 15-lipoxygenase (1993) *Science 260*, 1482-1486.

39. Jonsson, T., Glickman, M. H., Sun, S. J., and Klinman, J. P.Experimental evidence for extensive tunneling of hydrogen in the lipoxygenase reaction: implications for enzyme catalysis (1996) *J. Am. Chem. Soc. 118*, 10319-10320.

40. Glickman, M. H., Wiseman, J. S., and Klinman, J. P. Extremely Large Isotope Effects in the soybean lipoxygense-linoleic acid reaction (1994) *J. Am. Chem. Soc. 116*, 793-794.

41. Glickman, M. H., and Klinman, J. P. Lipoxygenase reaction mechanism: demonstration that hydrogen abstraction from substrate precedes dioxygen binding during catalytic turnover (1996) *Biochemistry 35*, 12882-12892.

42. Glickman, M. H., and Klinman, J. P. Nature of rate-limiting steps in the soybean lipoxygenase-1 reaction (1995) *Biochemistry 34*, 14077-14092.

	WT	**Trpt500Phe**	**Trp500Leu**	**Arg707Leu**	**Lys260Leu**
	HPOD	***HPOD***	***HPOD***	***HPOD***	***HPOD***
K_D (μM) *activation*	26.5+/-.8	34+/-8	81+/-12	189+/-17	19.6+/-6
k_2 (s^{-1})	180+/-6	387+/-30	542+/-36	34.5+/-5.5	292+/-24
	WT	**Trpt500Phe**	**Trp500Leu**	**Arg707Leu**	**Lys260Leu**
	HPETE	***HPETE***	***HPETE***	***HPETE***	***HPETE***
K_D (μM) *activation*	49+/-5	44+/-5	46+/-10	491+/-112	58.3+/-5.8
k_2 (s^{-1})	402+/-17	390.5+/-13	318+/-32	69+/-8	387+/-43

TABLE 1a. Dissociation constants (K_D) and rate constants (k_2) for the activation of soybean lipoxygenase (Fe^{II}) with HPOD and HPETE for WT, Trp500Phe, Trp500Leu, Arg707Leu, and Lys260Leu.

	WT	Trpt500Phe	Trp500Leu	Arg707Leu	Lys260Leu
	HPOD	***HPOD***	***HPOD***	***HPOD***	***HPOD***
K_D (μM) purple lipoxygenase	31.3+/-3.6	49.8+/-1.9	87.2+/-2.3	160+/-15	39.1+/-5.8

TABLE 1b. Dissociation constants (K_D) Fe^{III}-HPOD-purple lipoxygenase complex for WT, Trp500Phe, Trp500Leu, Arg707Leu, and Lys260Leu.

	WT/LA	Trp500Phe/LA	Trp500Leu/LA	Arg707Leu/LA	Lys260Leu/LA
k_{cat} (s^{-1})	276+/-22	249+/-19	132+/-3	174+/-11	288+/-18
k_{cat}/K_m	21.0 +/-3.6	24.2+/-2.8	16.0+/-3.2	8.9+/-1.3	23.2+/-4.0
	WT/AA	**Trp500Phe/AA**	**Trp500Leu/AA**	**Arg707Leu/AA**	**Lys260Leu/AA**
k_{cat} (s^{-1})	434+/-14	495+/-10	221+/-10	370+/-5	454+/-22
k_{cat}/K_m	38.1+/-4.0	43.5+/-2.8	41.0+/-7.1	18.5+/-2	26.1+/-3.0

TABLE 2. Kinetic parameters (k_{cat}/K_m^H, k_{cat}^H (s^{-1})) for WT, Trp500Phe, Trp500Leu, Arg707Leu, and Lys260Leu with LA and AA as substrates.

	LA	AA	HPOD	15-(S)-HPETE
WT	-10.23	-12.09	-10.52	-12.72
Arg707Leu	-6.30	-8.80	-6.31	-7.19

TABLE 3. GLIDE scores for LA, AA, HPOD, and 15-(S)-HPETE bound to WT and Arg707Leu. A more negative glide score indicates a better fit in the binding site.

SCHEME1: Bond formation between HPOD and SLO (Fe^{III}) to form purple lipoxygenase.

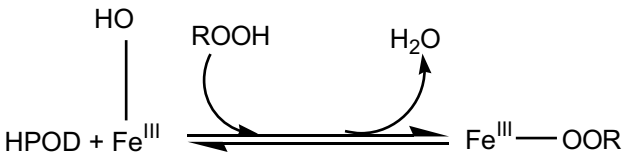

FIGURE 1a. Binding of LA, “carboxylate-end (hydrophilic) first”, with the double bond/tryptophan and the argenine/carboxylic acid end interaction.

FIGURE 1b. Binding of LA, “methyl-end (hydrophobic) first”, with the double bond/tryptophan and the lysine/carboxylic-acid-end interaction.

FIGURE 2. Activation of WT (◊), Trp500Phe (■), Trp500Leu (▲), Arg707Leu (X), and Lys260Leu (○) with HPOD . Formation of Fe^{III} is followed via fluorescence.

FIGURE 3. Images of products docked in the WT sLO-1 binding site using GLIDE.

FIGURE 4a. Energy diagram for the oxidation step in the activation of WT versus Trp500Leu.

FIGURE 4b. Energy diagram for the oxidation step in the activation of WT versus Arg707Leu.

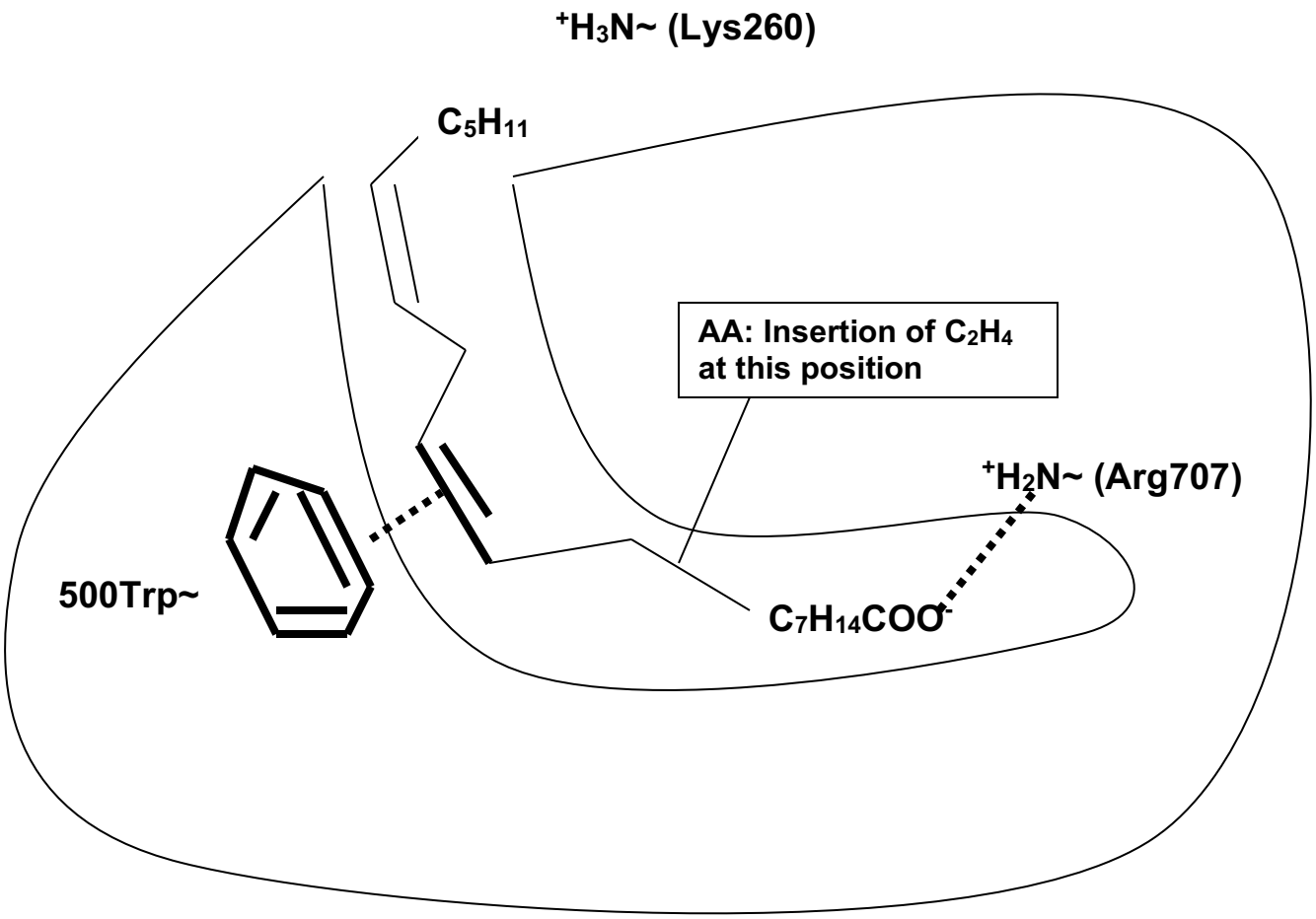
+H3N~ (Lys260)
C5H11
AA: Insertion of C2H4
at this position
+H2N~ (Arg707)
500Trp~
C7H14COO-

FIGURE 1a

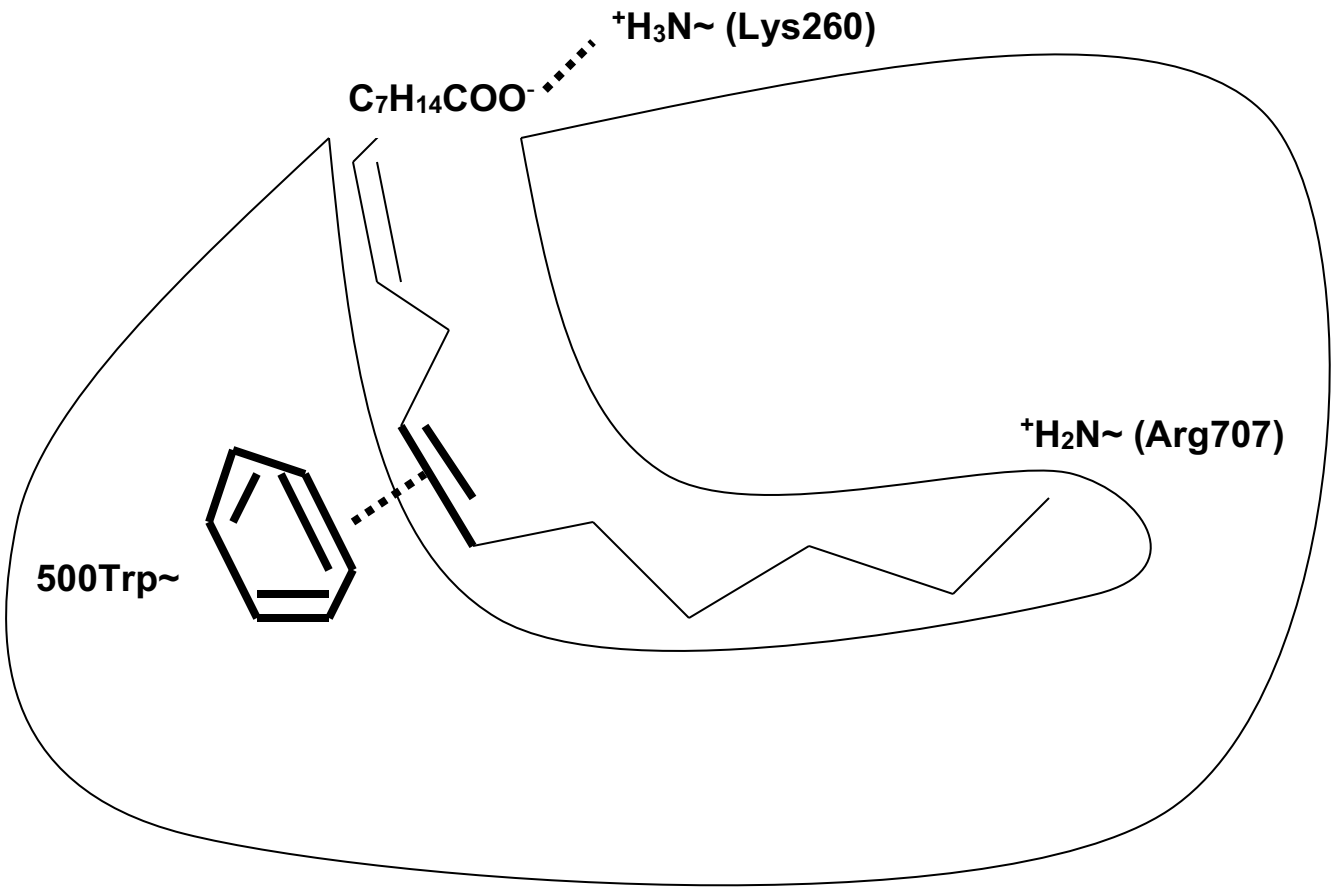

FIGURE 1b

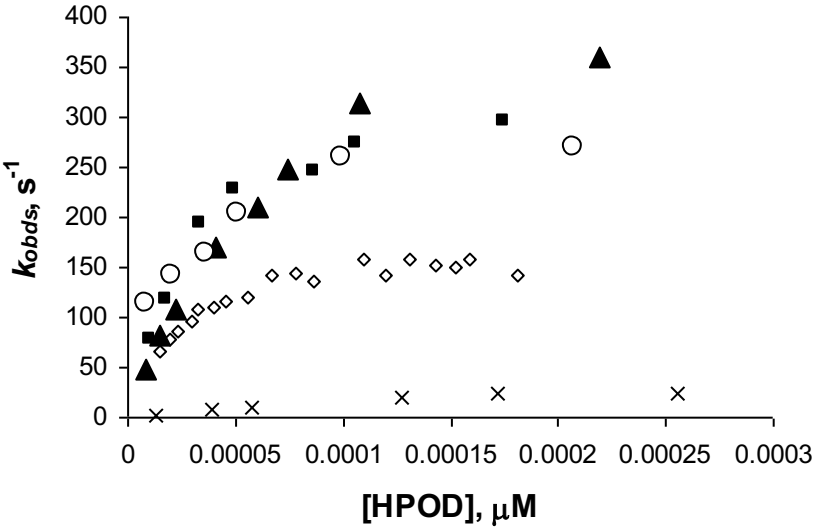
400
350
300
250
200
150
100
50
0
k_{obds}, s^{-1}
0
0.00005
0.0001
0.00015
0.0002
0.00025
0.0003
[HPOD], μM

FIGURE 2

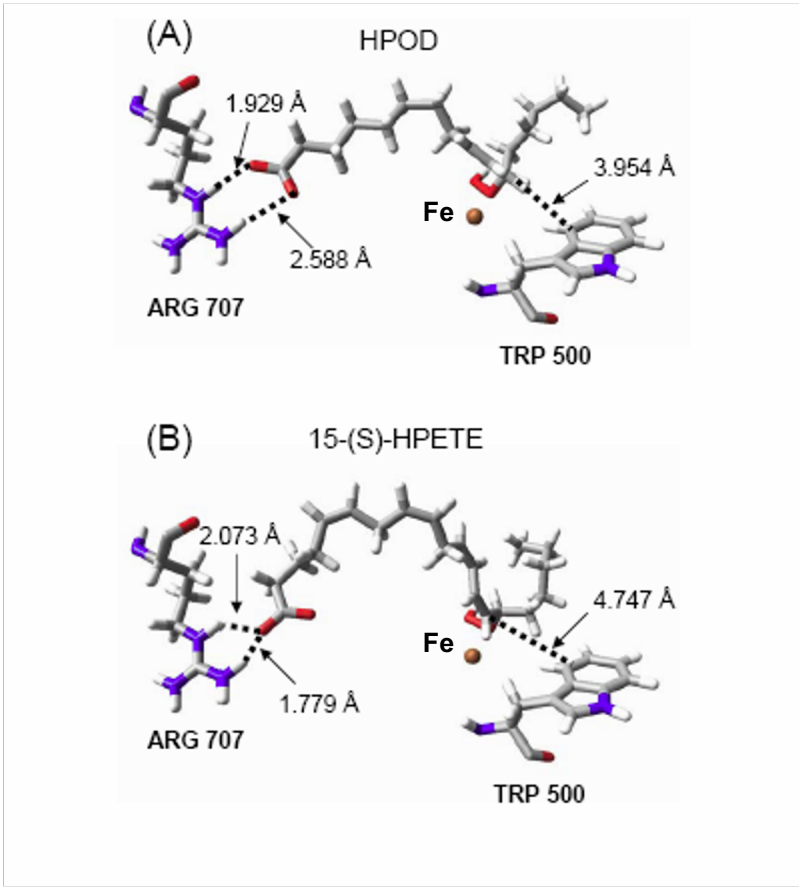
(A)
HPOD
1.929 Å
3.954 Å
Fe
2.588 Å
ARG 707
TRP 500
(B)
15-(S)-HPETE
2.073 Å
4.747 Å
Fe
1.779 Å
ARG 707
TRP 500

FIGURE 3

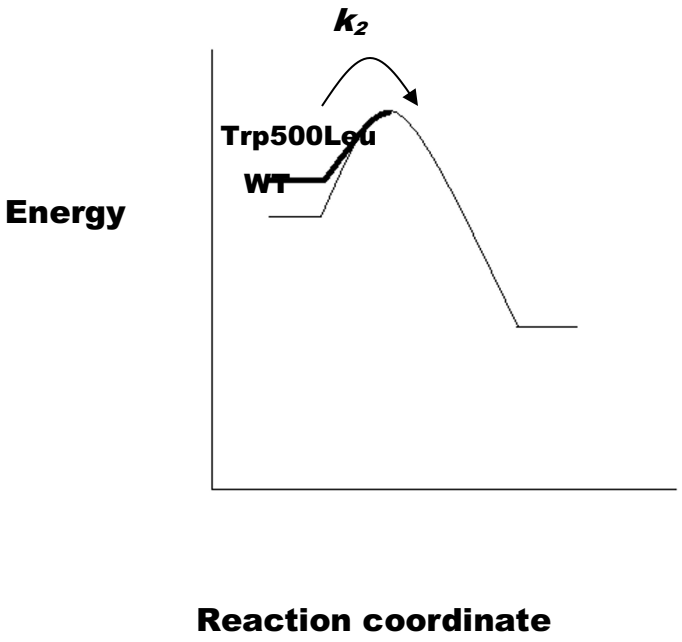

FIGURE 4a

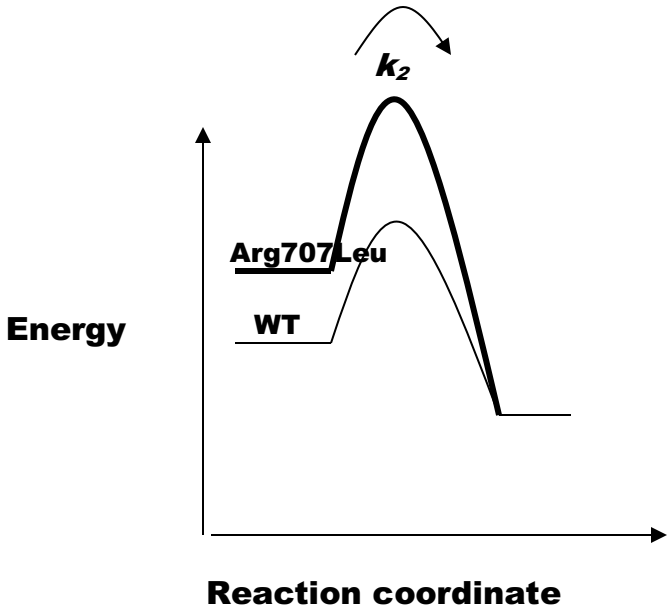

FIGURE 4b

For Table of Contents Only:

Tryptophan 500 and Arginine 707 Define Product and Substrate Active Site Binding in Soybean Lipoxygenase-1

Defining the soybean lipoxygenase binding site

Viola C. Ruddat[&], Rakesh Mogul[&], Ilya Chorny[#], Cameron Chen[&], Noah Perrin[&], Stephanie Whitman[&], Victor Kenyon[&], Matthew P. Jacobson[#], Claude F. Bernasconi[&] and Theodore R. Holman[&*]